Investigating the inner discs of Herbig Ae/Be stars with CO bandhead and Brγ emission[★]

J. D. Ilee,[1]† J. Fairlamb,[2] R. D. Oudmaijer,[2] I. Mendigutía,[2] M. E. van den Ancker,[3] S. Kraus[4] and H. E. Wheelwright[5]

[1]*SUPA, School of Physics and Astronomy, University of St Andrews, North Haugh, St Andrews, Scotland KY16 9SS, UK*
[2]*School of Physics and Astronomy, EC Stoner Building, University of Leeds, Leeds LS2 9JT, UK*
[3]*European Southern Observatory (ESO), Karl-Schwarzschild-Str. 2, D-85748 Garching, Germany*
[4]*School of Physics, University of Exeter, Stocker Road, Exeter EX4 4QL, UK*
[5]*Max-Planck-Institut für Radioastronomie, Auf dem Hügel 69, D-53121 Bonn, Germany*

ABSTRACT

Herbig Ae/Be stars lie in the mass range between low- and high-mass young stars, and therefore offer a unique opportunity to observe any changes in the formation processes that may occur across this boundary. This paper presents medium-resolution Very Large Telescope (VLT)/X-shooter spectra of six Herbig Ae/Be stars, drawn from a sample of 91 targets, and high-resolution VLT/Cryogenic Infrared Echelle Spectrograph (CRIRES) spectra of five Herbig Ae/Be stars, chosen based on the presence of CO first overtone bandhead emission in their spectra. The X-shooter survey reveals a low detection rate of CO first overtone emission (7 per cent), consisting of objects mainly of spectral type B. A positive correlation is found between the strength of the CO $v = 2$–0 and Brγ emission lines, despite their intrinsic linewidths suggesting a separate kinematic origin. The high-resolution CRIRES spectra are modelled, and are well fitted under the assumption that the emission originates from small scale Keplerian discs, interior to the dust sublimation radius, but outside the corotation radius of the central stars. In addition, our findings are in very good agreement for the one object where spatially resolved near-infrared interferometric studies have also been performed. These results suggest that the Herbig Ae/Be stars in question are in the process of gaining mass via disc accretion, and that modelling of high spectral resolution spectra is able to provide a reliable probe into the process of stellar accretion in young stars of intermediate to high masses.

Key words: circumstellar matter – stars: emission-line, Be – stars: formation – stars: massive – stars: pre-main-sequence – infrared: stars.

1 INTRODUCTION

Circumstellar discs surrounding young stellar objects (YSOs) have been the focus of much research because not only do they provide the location for possible planet formation to occur, but they play an essential role in the regulation and evolution of the accretion that takes place during the star formation process (see the review of Turner et al. 2014). Pre-main-sequence Herbig Ae and Be stars (HAeBes; see Waters & Waelkens 1998) lie in the mass range between lower mass T Tauri stars ($M_\star < 2$ M$_\odot$) and short-lived,

obscured massive young stellar objects (MYSOs; $M_\star > 8$ M$_\odot$). Thus, they offer a unique opportunity to observe and characterize any similarities or differences between low- and high-mass star formation processes (see Larson 2003; McKee & Ostriker 2007 for reviews). For example, across the mass range between T Tauri stars and MYSOs, there is evidence for a change in the mechanism that transfers material from the surrounding natal cloud, through the disc, and on to the central protostar. The mechanism is thought to switch from T Tauri-like magnetospheric accretion – in which the disc is truncated at radial distances no larger than the corotation radius and accretion proceeds to the stellar surface via magnetically channelled accretion funnels (Bertout 1989; Bouvier et al. 2007) – to some other, as yet uncharacterized phenomenon (Vink et al. 2003, 2005). The reason for this possible change in accretion mechanism is because the interior envelopes of HAeBes are thought to be mostly radiative in nature (Hubrig et al. 2009). Therefore, they lack

the interior convection currents required to power strong magnetic fields – a requirement for such magnetospheric accretion to occur. Recent observations show a low detection rate of magnetic fields (~7 per cent) across a large sample of HAeBes, supporting this scenario (Alecian et al. 2013). It is possible that the lower mass Herbig Ae stars undergo similar magnetospheric accretion to that of T Tauri stars (Muzerolle et al. 2004; Mottram et al. 2007), but the situation for the higher mass Herbig Be stars is not known.

An alternative to magnetospheric accretion is direct accretion (also called boundary layer accretion), where material from the disc is accreted directly on to the stellar surface, along the ecliptic plane (Lynden-Bell & Pringle 1974; Bertout, Basri & Bouvier 1988; Blondel & Tjin A Djie 2006). For boundary layer accretion to occur, a disc-like geometry would have to be present on scales smaller than the corotation radius of the star – the location at which any magnetospheric accretion funnels would likely begin to operate (Shu et al. 1994; Muzerolle et al. 2003). Therefore, in order to investigate the accretion mechanisms of these young stars, information on the geometry of inner regions of the circumstellar disc, close to the central star is required.

While it is believed that dust is responsible for most of the thermal emission from circumstellar discs, it is likely that gas is responsible for the majority of their mass. HAeBes possess strong stellar radiation fields compared to that of their lower mass counterparts. Because of this, regions of their circumstellar discs close to the central star are likely to be heated to high temperatures. If this temperature exceeds the dust sublimation temperature, then the dust in the disc is destroyed. This gives rise to an inner disc consisting of only gas, out to the location of the dust sublimation radius, on scales of a few astronomical units (see the review of Dullemond & Monnier 2010).

Direct observations of these regions of HAeBes are complicated by the fact that most objects lie at relatively large distances. Thus, the small sizes of the regions involved mean that imaging is only possible using interferometry. However, this is an observationally complex task limited to bright targets (Kraus et al. 2008a; Tatulli et al. 2008; Wheelwright et al. 2012). Therefore, there is much interest in determining more indirect observational techniques that can probe the conditions close to the central star.

The most abundant molecule in circumstellar discs is molecular hydrogen (H_2). However, the large energies required to excite H_2, low transition probabilities and atmospheric absorption across the relevant wavelength range mean that thermal emission from this molecule is difficult to observe, and it is therefore not an efficient tracer of these regions. Coupled rotational and vibrational emission of the next most abundant molecule, CO, offers an alternative diagnostic. CO bandhead emission (also called overtone emission) is excited in warm ($T = 2500$–5000 K) and dense ($n > 10^{15}$ cm^{-3}) neutral gas – exactly the conditions expected in the inner parts of accretion discs, making this emission a valuable probe of these regions (Glassgold, Najita & Igea 2004). Several previous investigations have been successful in fitting the CO bandhead spectra of young stars under the assumption that the emission originates from a gaseous circumstellar disc (Carr 1989; Bik & Thi 2004; Blum et al. 2004; Thi et al. 2005; Wheelwright et al. 2010; Cowley et al. 2012; Ilee et al. 2013).

The $n = 7$–4 transition of atomic hydrogen (H I) in the Brackett series (Brγ) occurs at $\lambda = 2.16$ µm, and is also excited at high temperatures ($T \gtrsim 10^4$ K). The origin of such hydrogen recombination emission is still unknown. Several theories have been proposed, including magnetospheric accretion phenomena (Muzerolle, Calvet & Hartmann 1998a), inner disc regions (Muzerolle et al. 2004),

stellar winds (Strafella et al. 1998) and disc winds (Ferreira 1997). Muzerolle, Hartmann & Calvet (1998b) found that the Brγ line luminosity in a sample of low-mass (0.2–0.8 M$_\odot$) T Tauri stars was tightly correlated with the accretion luminosity as measured from blue continuum excess. Calvet et al. (2004) extended this investigation to YSOs with masses up to 4 M$_\odot$, and find good agreement with the previous study, and the relationship was used to examine the accretion rates of 36 Herbig Ae stars by Garcia Lopez et al. (2006). More recently, Mendigutía et al. (2011) determined accretion luminosities from 38 HAeBes by examining the ultraviolet (UV) excess in the Balmer discontinuity, and found a correlation with Brγ luminosity similar to Calvet et al. (2004).

This paper utilizes a collection of Very Large Telescope (VLT) X-shooter and Cryogenic Infrared Echelle Spectrograph (CRIRES) observations of several Herbig Ae/Be objects based on the detection of CO first overtone bandhead emission in their spectra. The observations, sample selection and determination of stellar parameters are described in Section 2. The measured observable quantities are presented and analysed in Section 3. Modelling of the CO spectra is discussed, and comments on individual objects are given in Section 4. Discussion of the results from both sets of observations is presented in Section 5, and finally conclusions are outlined in Section 6.

2 OBSERVATIONS AND SAMPLE SELECTION

The observations for this investigation were obtained using two instruments on the ESO VLT at Cerro Paranal. High-resolution 2.3 µm spectra of five Herbig Ae/Be stars, targeted because of previous detection of CO first overtone bandhead emission, were obtained using the cryogenic spectrograph CRIRES (Käufl et al. 2008). The CRIRES observations of HD 36917, HD 259431 and HD 58647 were taken on 2010 October 26 and 27. Using a slit width of 0.2 arcsec, the observations achieved spectral resolution of approximately 80 000. The observations of PDS 37 were taken on 2007 June 6 and originally published in Ilee et al. (2013). Using a slit width of 0.6 arcsec, a spectral resolution of approximately 30 000 was achieved. The archival observations of HD 101412 were taken on 2011 April 5, and were originally published by Cowley et al. (2012). Using a slit width of 0.2 arcsec, this achieved a spectral resolution of over 90 000. Telluric line removal for all CRIRES observations was performed using standard stars at comparable airmasses, obtained during the same observing run as the science observations.

In addition to the targeted CRIRES observations, a medium-resolution spectroscopic survey was performed using the cross-dispersed wide band spectrograph X-shooter (Vernet et al. 2011). A total of 91 objects were observed in service mode between 2009 October and 2010 March (Oudmaijer et al. 2011; Fairlamb et al., in preparation). X-shooter provides simultaneous wavelength coverage from 300 to 2480 nm using three spectrograph arms – UV (UVB), visible (VIS) and near-infrared (NIR). The original sample of 91 Herbig Ae/Be stars was taken from the catalogues of Thé, de Winter & Perez (1994) and Vieira et al. (2003), and was selected based on sky coordinates appropriate for the observing semester. A small number were discarded due to insufficient brightness or ambiguous assignment as a HAeBe star. This sample is larger than most other published studies by a factor of 2–5. In addition to the large sample size, the use of X-shooter allows comparison of many spectral features from a single observation, which is important given that HAeBes have been shown to be both photometrically and spectrally variable (Oudmaijer et al. 2001). This paper utilizes data from the

Table 1. Log of the observations performed with VLT/X-shooter and VLT/CRIRES in which CO first overtone emission was detected. Signal-to-noise ratio (S/N) is measured in featureless regions around 2.28 μm.

Object	Other name	RA (J2000)	Dec. (J2000)	Instrument	S/N	t_{exp} (h)	Date
HD 36917		05:34:47.00	−05:34:10.5	CRIRES	270	0.2	2010-10-26
HD 259431	MWC 147	06:33:04.90	+10:19:20.3	CRIRES	172	0.2	2010-10-26
HD 58647		07:25:56.10	−14:10:45.8	CRIRES	208	0.3	2010-10-27
PDS 37	Hen 3−373	10:10:00.32	−57:02:07.3	CRIRES	114	0.1	2007-06-06
HD 101412	V1052 Cen	11:39:44.46	−60:10:27.9	CRIRES	150	0.2	2011-04-05
HD 35929		05:27:42.79	−08:19:38.6	X-shooter	68	0.03	2009-12-17
PDS 133	SPH 6	07:25:04.95	−25:45:49.7	X-shooter	51	0.30	2010-02-24
HD 85567	V596 Car	09:50:28.53	−60:58:03.0	X-shooter	123	0.02	2010-03-06
PDS 37	Hen 3−373	10:10:00.32	−57:02:07.3	X-shooter	115	0.03	2010-03-31
HD 101412	V1052 Cen	11:39:44.46	−60:10:27.9	X-shooter	72	0.06	2010-03-30
PDS 69	Hen 3−949	13:57:44.12	−39:58:44.2	X-shooter	48	0.03	2010-03-29

NIR arm, and deals mainly with the subset of six objects from the full sample that showed a detection of CO first overtone bandhead emission at 2.3 μm.

The observations using X-shooter achieved a spectral resolution of $R \sim 8000$ ($\Delta\lambda = 0.28$ nm at $\lambda = 2.3$ μm) using a slit width of 0.4 arcsec. A single pixel element covered 0.06 nm, while a resolution element covered 4.3 pixels. The atmospheric seeing conditions in the optical varied from 1.1 to 1.6 arcsec between observations. The exposure times ranged from several minutes for the brightest sources, up to 30 min for the faintest ones. Nodding along the slit was performed to allow background subtraction. The data were reduced with version 0.9.7 of the ESO pipeline software (Modigliani et al. 2010), and verified with manually reduced data for a handful of objects to ensure consistency. The data were of high quality, with signal-to-noise ratios of 100–140 in most cases across the entire sample of HAeBes.

To correct telluric absorption features within the X-shooter spectra, the ESO software MOLECFIT[1] was used (Kausch et al., in preparation; Smette et al., in preparation). The MOLECFIT program models the atmospheric absorption above the telescope using temperature, pressure and humidity profiles for the observing site, a radiative transfer code and a data base of molecular parameters. We used the code to accurately model the atmospheric absorption features in the telluric observations themselves. This then produced model telluric spectra tuned to the exact atmospheric conditions measured on the night of the observation, but free from the effects of noise. These model spectra were then used to remove telluric features from the science observations, which resulted in a better correction than was possible using the standard stars alone.

A log of the observations of these objects is shown in Table 1, their spectra around the CO first overtone and Brγ region are shown in Figs 1 and 2 and their astrophysical parameters are given in Table 2.

2.1 Determining stellar parameters

Stellar parameters for the targets observed with CRIRES were taken from various sources in the literature (see Table 2). Stellar parameters for the X-shooter sample were determined directly using two methods that will be described in detail by Fairlamb et al. (in preparation), but here we briefly summarize the approach. The first method involved calculating the temperature and surface
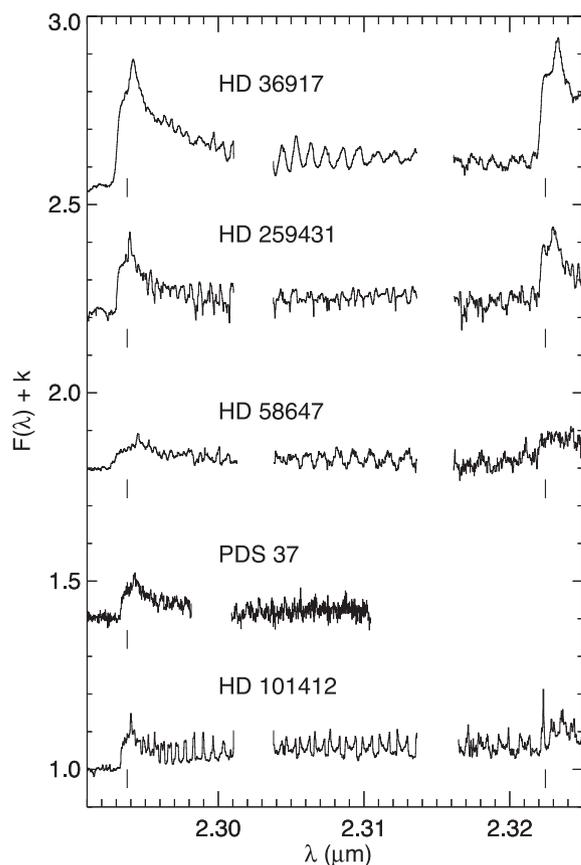
[1] http://www.eso.org/sci/software/pipelines/skytools/molecfit

Figure 1. VLT/CRIRES spectra of the sample of objects showing CO first overtone bandhead emission. Spectra have been normalized to the continuum and shifted vertically for clarity. Vertical ticks mark the rest wavelengths of the CO $v = 2$–0 and 3–1 transitions, respectively. The observations of PDS 37 were conducted using an alternative wavelength setting to the rest of the observations, therefore, no data are available beyond 2.311 μm.

gravity, log g, of the objects by adopting a similar method to that of Montesinos et al. (2009). A best fit was performed across the hydrogen recombination lines of the Balmer series (Hβ, Hγ and Hδ) between the observed X-shooter spectra and a grid of Kurucz–Castelli models (Kurucz 1993; Castelli & Kurucz 2004). The fit was made specifically to the wings of the recombination lines, as
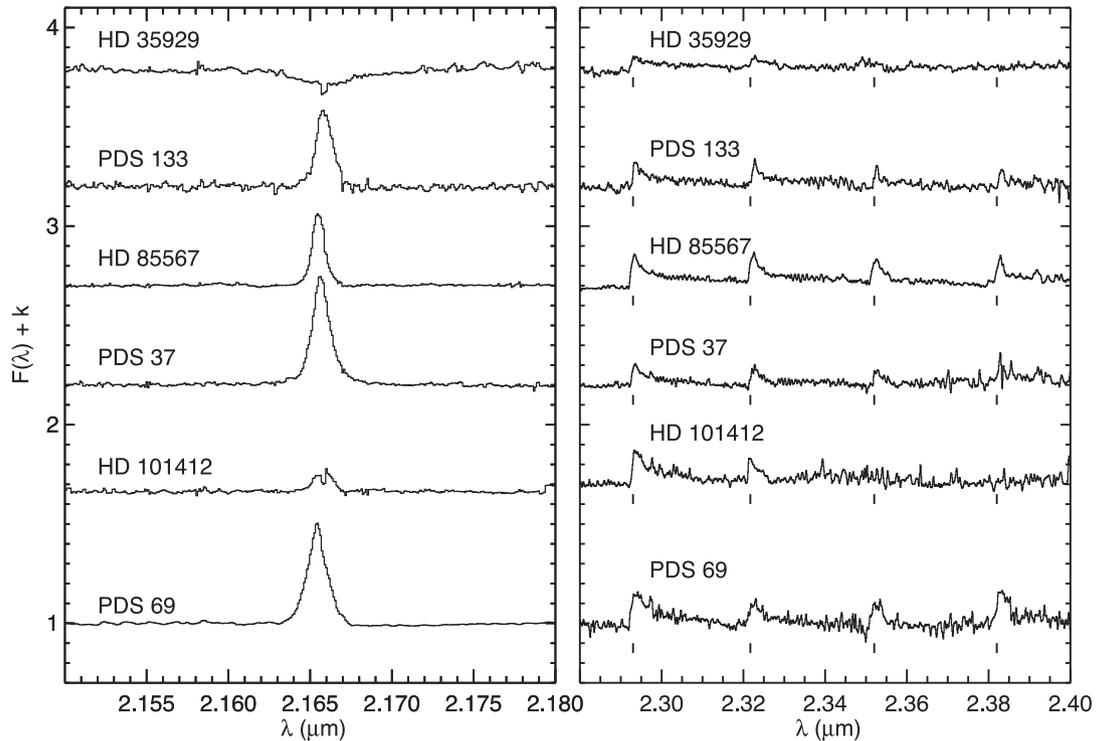
Figure 2. VLT/X-shooter spectra of the sample of objects from Table 1 across the Brγ (left) and CO first overtone (right) wavelength ranges. Spectra have been normalized to their respective continuum, shifted vertically for clarity, and re-binned by a factor of 2 to reduce the effect of noise. In the right-hand panel, vertical ticks mark the rest wavelengths of the CO v = 2–0, 3–1, 4–2 and 5–3 transitions, respectively.

Table 2. Astrophysical parameters of the sample that have been adopted for this work. Stellar parameters are determined as described in Section 2.1 unless otherwise stated. Dust sublimation radii are calculated with equation (1). K-band magnitudes are taken from 2MASS (Skrutskie et al. 2006).

Object	Spectral type	K (mag)	d (pc)	$T_{\rm eff}$ (K)	A_V (mag)	$\log L_{\rm bol}$ ($L_\odot$)	$M_\star$ ($M_\odot$)	$R_\star$ ($R_\odot$)	$R_{\rm sub}$ (au)	$v\sin i$ (km s^{-1})	$R_{\rm cor}$ (au)
HD 36917	B9.5e[a]	5.7	470[a]	10 000[a]	0.5[b]	2.20[b]	2.5[a]	1.8[a]	0.4	125[b]	0.02
HD 259431	B6e[c]	5.7	800[c]	14 125[c]	1.2[c]	3.19[c]	6.6[c]	6.63[c]	3.3	100[d]	0.07
HD 58647	B9e[e]	5.4	277[e]	10 500[f]	1.0	2.95[f]	3.0[e]	2.8[e]	0.8	118[g]	0.03
PDS 37	B2e[h]	7.0	720[h]	22 000[h]	5.66	3.27	7.0	3.0	3.8	. . .	. . .
HD 101412	A0III/IVe[i]	7.5	395 ± 65	9750 ± 250	0.39	1.58	2.3	2.2	0.5	8[j]	0.15
HD 35929	F2IIIe[m]	6.7	325 ± 60	7000 ± 250	0.10	1.67	2.7	4.6	0.5	70[m]	. . .
PDS 133	B6e[h]	9.3	2270 ± 500	13 250 ± 1000	1.61	2.16	3.2	2.4	1.0	. . .	. . .
HD 85567	B7–8Ve[k]	5.8	470 ± 220	12 500 ± 1000	0.76	2.48	3.8	3.9	1.5	50[n]	. . .
PDS 69	B4Ve[l]	7.2	645 ± 120	16 500 ± 750	1.49	2.81	4.7	3.2	2.2	. . .	. . .

Notes: [a]Manoj et al. (2002); [b]Hamaguchi, Yamauchi & Koyama (2005); [c]Kraus, Preibisch & Ohnaka (2008b); [d]Hillenbrand et al. (1992); [e]Brittain et al. (2007); [f]Montesinos et al. (2009); [g]Mora et al. (2001); [h]Vieira et al. (2003); [i]Guimarães et al. (2006); [j]van der Plas et al. (2008); [k]van den Ancker, de Winter & Tjin A Djie (1998); [l]Reipurth & Zinnecker (1993); [m]Miroshnichenko et al. (2004); [n]Miroshnichenko et al. (2001).

their broadness is sensitive to changes in temperature and surface gravity. Only the flux measurements above a level of 0.8 of the normalized continuum were included, to avoid contamination of the fit by any emission component. These temperature and surface gravity values were then compared against the PARSEC pre-main-sequence evolutionary tracks models (Bressan et al. 2012), which provided a corresponding stellar mass, radius and luminosity.

However, only half of the objects in the sample could be constrained using this method, due to extreme emission of the Balmer series which eclipses even the broad wings, and often other strong emission lines were present complicating any temperature estimate. For these objects, known photometry from the literature was used to determine a luminosity for the objects. Then the Kurucz–Castelli models were fit to the photometry by reddening each model until

a best-fitting slope was found, providing a temperature and surface gravity. A range of distances were then tested to provide a luminosity and radius, and from the surface gravity a mass was determined. A cross-comparison of these parameters was then made with the PARSEC tracks, where for each temperature and luminosity pair there was a unique mass and radius. This then gave a luminosity that with matching parameters between both the PARSEC tracks and the photometry fit. Both of the methods described above were tested for consistency on a handful of objects, and produced very similar stellar parameters. The stellar parameters of the object PDS 37 proved difficult to determine using the methods above, so the distance and luminosity were fixed to literature values (Vieira et al. 2003), which allowed a mass, radius, temperature and luminosity to be determined.

Estimation of the typical sizes of important physical regions was also carried out for each object – specifically the location of the dust sublimation radii, $R_{\rm sub}$, and the corotation radii, $R_{\rm cor}$. One of the most simple approaches in estimating $R_{\rm sub}$ is an analytic prescription, such as those described in Tuthill, Monnier & Danchi (2001) and Monnier & Millan-Gabet (2002). Such approaches are based on the assumptions about the absorption efficiencies of the dust in the disc, and using these assumptions to calculate the radius at which dust would survive given a certain stellar luminosity. However, these calculations neglect second-order effects, such backwarming of the disc material through reradiation of the stellar heating from the dust grains, or the effect of non-homogenously sized grains. Addressing such effects requires a proper treatment of radiative transfer. Whitney et al. (2004) calculated a series of two-dimensional radiative transfer simulations of discs around young stars, with effective temperatures up to 3×10^4 K. Their models include the effect of reradiation, and use a distribution of dust grain sizes based on the description in Wood et al. (2002), with sizes between 0.01 and 1000 µm. From the results of these simulations, the authors determined an analytic relationship between the dust sublimation radius and the stellar effective temperature of

$$R_{\rm sub} = R_\star \left(\frac{T_{\rm sub}}{T_\star} \right)^{-2.085}, \tag{1}$$

where $T_{\rm sub}$ is the temperature at which the dust sublimates. By assuming $T_{\rm sub}$ is 1500 K, we have used this relation along with the stellar effective temperatures in order to calculate the dust sublimation radii of our objects, which are shown in Table 2. However, it seems worthwhile to note that it is difficult to assign a single value to $R_{\rm sub}$ – different dust species will likely survive to different temperatures based on their composition, and in reality the dust sublimation will take place across a range of radii in the disc. Nonetheless, as we are simply estimating the size of typical regions within the discs, such treatment is beyond the scope of this investigation.

Where available in the literature, measured $v \sin i$ values were obtained and used together with the derived disc inclinations from the CO bandhead fitting (see Section 4), in order to determine the stellar angular velocity ω. This was then used to determine the corotation radii,

$$R_{\rm cor} = \left(\frac{GM_\star}{\omega^2} \right)^{1/3}, \tag{2}$$

of the objects, which are shown in Table 2.

3 OBSERVATIONAL RESULTS

From the sample of 91 Herbig Ae/Be stars taken with X-shooter, we investigate two NIR emission features – Brγ and the CO first overtone bandheads. The equivalent widths (W) and full width at half-maximum (FWHM) of both lines were measured using the IRAF NOAO/ONEDSPEC package. For each object, 10 measurements were taken, and an average of these was reported as the final result, with the error in this value given as the standard deviation of these measurements.

Because many A- and B-type stars exhibit photospheric Brγ absorption, the equivalent widths for the Brγ lines needed to be corrected for this effect. We adopted a method similar to Garcia Lopez et al. (2006), with the expression

$$W({\rm Br}\gamma)_{\rm circ} = W({\rm Br}\gamma)_{\rm obs} - W({\rm Br}\gamma)_{\rm phot}\, 10^{-0.4\Delta K}, \tag{3}$$

where $W({\rm Br}\gamma)_{\rm obs}$ is the observed equivalent width, $W({\rm Br}\gamma)_{\rm phot}$ is the equivalent width of the corresponding Kurucz–Castelli stellar

spectra based on spectral type of the object and ΔK is the disc continuum emission, computed by subtracting the observed K magnitude from the photospheric K magnitude of the corresponding model at the same given distance. After performing the correction for photospheric absorption, Brγ emission was detected in 64 objects in the sample, absorption was detected in six, 21 sources did not show detections (where we define non-detection for the Brγ line as sources which show $-1 < W_{\rm circ} < 1$ Å).

Six objects exhibited CO first overtone emission (HD 35929, PDS 133, HD 85567, PDS 37, HD 101412 and PDS 69), and the remaining 85 objects did not show detections above a 3σ level across the $v = 2$–0 transition. This subset of six stars showing detections of CO overtone emission in the X-shooter sample forms the basis of the subsequent analysis in this work, and their spectra across the wavelength range including Brγ and CO overtone are shown in Fig. 2. The objects PDS 133, HD 85567, PDS 37 and PDS 69 all show emission from the $v = 2$–0, 3–1, 4–2 and 5–3 vibrational transitions, while the objects HD 35929 and HD 101412 only show emission across the $v = 2$–0 and 3–1 transitions.

The detection rate of Brγ emission is 70 per cent, which is similar to other studies of lower mass T Tauri stars (74 per cent; Folha & Emerson 2001). The detection rate of CO first overtone emission is 7 per cent, which is lower than other studies of CO bandhead emission in young stellar objects, where detection rates of around 20 per cent have been reported in low- to intermediate-mass YSOs (e.g. Carr 1989; Connelley & Greene 2010) and 17 per cent for massive YSOs (e.g. Cooper et al. 2013).

The line flux is calculated from the product of the equivalent width of the emission line (in the case of Brγ we use the circumstellar component $W_{\rm circ}$) and the extinction corrected flux of the object in the K band (where we take $A_K = 0.11\, A_V$; Cardelli, Clayton & Mathis 1989). Examination of the near- to far-infrared continuum fluxes of each object suggested that a extrapolation of the K-band magnitude to 2.16 and 2.3 µm is appropriate to determine the line fluxes for both Brγ and CO. Line luminosities were then calculated using the distances determined in Section 2.1, where all measurements and corresponding errors are shown in Table 3.

For the CO first overtone emission, the strongest emission relative to the continuum is detected in PDS 69, while the weakest is in HD 35929 (the only star of spectral type F with a CO detection in our sample). The strongest Brγ emission relative to the continuum is observed in PDS 37, while the weakest emission is detected in HD 101412. While most of the Brγ emission is single peaked, we also observe double-peaked emission in the spectrum of HD 101412. The objects displaying single-peaked Brγ emission (PDS 133, HD 85567, PDS 367 and PDS 69) also show other hydrogen recombination lines with similar line shapes – specifically single-peaked Hα and Paγ emission. HD 101412 shows a weak double peak in Hα and Paγ, located within a region of broad absorption. In contrast to the other objects, the Brγ line in HD 32929 appears to be in absorption with a very broad extent in Fig. 2, but after correction for the effect of photospheric absorption, we determine this line to be in emission. It should be noted that this object has also previously been classified as a post-main-sequence star (Miroshnichenko et al. 2004). A full study of the other atomic hydrogen lines mentioned here, and their diagnostic power will be performed in a subsequent publication (Fairlamb et al., in preparation).

Similarly to Brittain et al. (2007), the line shapes of the Brγ emission are broad (130–220 km s^{-1}) and do not exhibit a blueshifted absorption component often seen in Herbig Ae/Be stars, which suggests the emission does not originate in a wind. The Brγ emission

Table 3. Equivalent widths (W), line fluxes (F), line luminosities (L) and linewidths (FWHM) as measured for Brγ and CO $v = 2$–0 emission shown in Figs 1 and 2. Equivalent widths for Brγ are corrected for photospheric absorption using the method described in Section 3. Equivalent widths for CO are measured from 2.29 to 2.30 μm. Also shown is the mass accretion rate, $\dot{M}$, calculated based on the relationship described in equation (4).

Object	W(CO) (Å)	F(CO) (W m^{-2})	L(CO) (L$_\odot$)	FWHM(Brγ) (km s^{-1})	W(Brγ_{circ}) (Å)	F(Brγ) (W m^{-2})	L(Brγ) (L$_\odot$)	$\dot{M}$ (M$_\odot$ yr^{-1})
CRIRES								
HD 36917	-7.6 ± 0.2	$1.9 \pm 0.3 \times 10^{-15}$	-1.9 ± 0.3	...	...	...		...
HD 259431	-4.4 ± 0.1	$1.2 \pm 0.2 \times 10^{-15}$	-2.2 ± 0.4	...	-3.9 ± 0.3^b	$1.1 \pm 0.1 \times 10^{-15\,b}$	-2.1 ± 0.4	3.2×10^{-6}
HD 58647	-2.4 ± 0.2	$7.9 \pm 0.8 \times 10^{-15}$	-2.2 ± 0.1	...	-3.3 ± 0.3^b	$9.8 \pm 0.1 \times 10^{-16\,b}$	-1.7 ± 0.1	4.8×10^{-7}
HD 101412	-2.8 ± 0.3	$1.3 \pm 0.4 \times 10^{-16}$	-3.2 ± 0.4	...	...	...		...
PDS 37	-2.0 ± 0.4^a	$2.4 \pm 0.8 \times 10^{-16}$	-2.4 ± 0.3	...	...	...		...
X-shooter								
HD 35929	-2.4 ± 0.4	$2.2 \pm 0.4 \times 10^{-16}$	-1.7 ± 0.2	570 ± 90	-1.3 ± 0.9	$1.2 \pm 0.2 \times 10^{-16}$	-2.6 ± 0.2	1.5×10^{-7}
PDS 133	-4.0 ± 0.7	$4.0 \pm 0.7 \times 10^{-17}$	-2.2 ± 0.9	170 ± 5	-5.4 ± 0.5	$5.3 \pm 0.6 \times 10^{-17}$	-2.2 ± 0.9	1.3×10^{-6}
HD 85567	-4.7 ± 0.2	$1.1 \pm 0.1 \times 10^{-15}$	-1.6 ± 0.2	130 ± 2	-4.3 ± 0.1	$9.8 \pm 0.3 \times 10^{-16}$	-1.7 ± 0.2	1.2×10^{-6}
PDS 37	-3.0 ± 0.2	$3.7 \pm 0.3 \times 10^{-16}$	-2.9 ± 0.3	190 ± 6	-9.1 ± 0.9	$1.2 \pm 0.1 \times 10^{-15}$	-3.2 ± 0.5	1.3×10^{-6}
HD 101412	-5.1 ± 0.5	$2.4 \pm 0.2 \times 10^{-16}$	-3.1 ± 0.4	220 ± 20	-2.9 ± 0.4	$1.3 \pm 0.5 \times 10^{-16}$	-3.4 ± 0.4	1.3×10^{-7}
PDS 69	-6.7 ± 0.8	$4.6 \pm 0.6 \times 10^{-16}$	-2.2 ± 0.5	205 ± 15	-8.4 ± 0.6	$5.8 \pm 0.6 \times 10^{-16}$	-2.1 ± 0.5	9.1×10^{-7}

Notes: ^{a}Data do not extend across the full $v = 2$–0 bandhead, therefore, this value should be considered a lower limit.
^{b}Taken from Brittain et al. (2007), where we assume an error of 10 per cent.

of HD 101412 shows a double-peaked line profile, with a separation of 50 km s^{-1}. As the source of this double peaking is unknown, the FWHM is measured across the full width of the line, and should be considered a maximal value. The FWHM of each lobe of the emission corresponds to approximately 110 km s^{-1}. The FWHMs of the Brγ emission are approximately 5–10 times the thermal linewidth expected for hydrogen gas at the effective temperatures of the central protostars (20–30 km s^{-1}). This suggests the hydrogen recombination lines are broadened by non-thermal mechanisms, such as rotation, turbulence or in-fall towards the central star.

3.1 A relationship between CO bandhead and Br γ emission?

The relationship between the Brγ and CO first overtone is of interest, as both emission lines originate in circumstellar environments. In addition to the simultaneous X-shooter observations, the objects HD 259431 and HD 58647 for which we present CRIRES data are also shown to posses Brγ emission by Brittain et al. (2007). These fluxes are included in Table 3. However, it should be noted that because these data are not simultaneous, any effect of spectroscopic variability may alter the values slightly.

Fig. 3 shows the luminosities of both lines measured from the X-shooter and CRIRES data sets. The detections (filled and open circles) occupy the upper ranges of the relationship, showing that detection of CO overtone emission is associated with the detection of Brγ emission. The detections show a positive correlation, best fitted with the relationship $\log L(\text{CO}) = (0.6 \pm 0.2) \log L(\text{Br}\,\gamma) - (0.8 \pm 0.5)$. While this correlation does not imply a direct dependence on both of the emission lines, it suggests that similar factors may affect the strength of both lines when they are present.

As the calculation of upper limits for CO first overtone emission is complicated by the non-Gaussian shape of the overall feature, here we describe the process adopted to determine them. Using the modelling routine described in Section 4, a synthetic CO first overtone spectra is created, along with a spectrum of random noise. The strength of random noise is altered to produce a series of spectra that span the range of SNR shown by the observations (50–260). The strength of the CO emission is decreased until the peak of the $v = 2$–0 bandhead drops below the 3σ level in each of these spectra. The equivalent width is then measured across the 2.29–2.3 μm
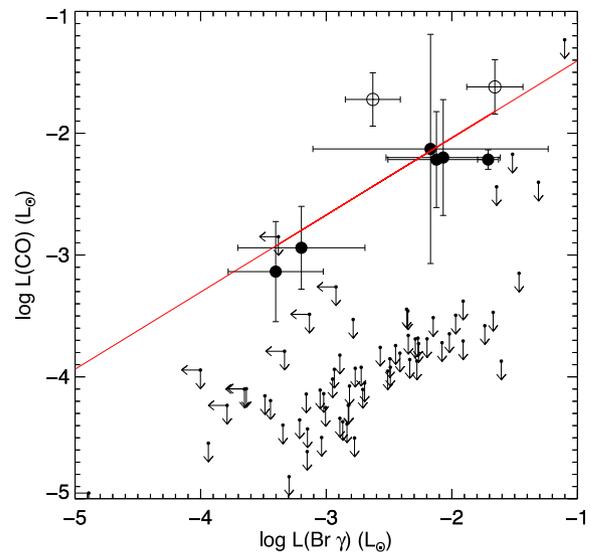

Figure 3. A comparison of the line luminosities measured from the CO $v = 2$–0 and Brγ lines (after correction for photospheric absorption) for objects displaying such lines in emission or with an upper limit for non-detection. Filled circles represent measurements from the simultaneous X-shooter observations, open circles represent non-simultaneous measurements from the CRIRES observations and literature data, and arrows represent measured upper limits for non-detections. A best fit to the detections, $\log L(\text{CO}) = (0.6 \pm 0.2) \log L(\text{Br}\,\gamma) - (0.8 \pm 0.5)$, is shown with a red line.

wavelength range for the corresponding model (with no random noise). The relationship between the true equivalent width and the SNR was then determined, and then used to calculated the upper limit of equivalent width for each non-detection, based on the SNR of the spectrum. The upper limits for non-detections were then taken as the product of the K-band flux density and this equivalent width, $F_{UL} = F_K W_{UL}$. To ensure consistency, we also perform an identical procedure for the non-detections of Brγ emission. However in this case, we use a Gaussian line shape centred at 2.1655 μm, rather than a model bandhead spectra.

Analysis of the non-detections shows that the upper limits for the line luminosities of CO first overtone emission are between 1 and

1.5 dex below the luminosities calculated from the detections. This suggests that our observations are not limited by noise in the spectra, and that more sensitive observations with longer integration times would not allow the detection of weaker CO first overtone emission following the same trend.

Given that the line luminosities in both axis of Fig. 3 were calculated by multiplying the equivalent widths by the same continuum fluxes and the same square distances to the corresponding objects (Section 2.1), we tested the possibility that the correlation is spurious. However, the Spearman's probability of false correlation does not significantly increase when both the continuum and distance values are considered through the partial correlation technique (Wall & Jenkins 2003). This suggests that the correlation between line luminosities is not spurious, although we note that more data are necessary to provide any statistical significance.

This correlation between the line luminosities is in agreement with several previous studies of both emission lines in young stars. Carr (1989) studied a sample of 40 YSOs, in which they find a positive correlation between the line luminosity of the CO $v = 2$–0 emission and the Brγ emission in the 10 objects with such emission. Connelley & Greene (2010) examined NIR spectra of 110 Class I YSOs, and found a positive correlation between the equivalent widths of the CO $v = 2$–0 and the Brγ lines, where detected in their sample.

3.2 Determining accretion rates

As mentioned previously, the luminosity of Brγ has been shown to correlate well with the accretion luminosity of intermediate-mass YSOs, giving rise to several correlations between the two quantities (see e.g. Calvet et al. 2004). Recently, Mendigutía et al. (2011) looked at a large sample of Herbig Ae stars and determined a correlation following:

$$\log \frac{L_{\mathrm{acc}}}{\mathrm{L}_{\odot}} = (0.91 \pm 0.27) \log \frac{L_{\mathrm{Br}\gamma}}{\mathrm{L}_{\odot}} + (3.55 \pm 0.80). \qquad (4)$$

We have used this correlation between accretion luminosity and Brγ line luminosity to determine the accretion luminosities of the objects possessing Brγ emission. Once the accretion luminosity has been determined, it is then used to calculate the mass accretion rate $\dot{M}$ via

$$\dot{M} = \frac{L_{\mathrm{acc}} R_{\star}}{G M_{\star}}. \qquad (5)$$

Table 3 shows the mass accretion rates that were determined for each object using this procedure (including the two objects where measurements were taken from Brittain et al. 2007). We also performed measurements of strength of Brγ emission for the remaining objects in the X-shooter observations.

The mass accretion rates of the all objects exhibiting Brγ emission span the range of 10^{-9}–10^{-4} M$_{\odot}$ yr^{-1}, with the majority of objects possessing rates of approximately 1×10^{-7} M$_{\odot}$ yr^{-1}. The mass accretion rates of the objects exhibiting both Brγ and CO first overtone emission span a smaller range of 10^{-7}–10^{-6} M$_{\odot}$ yr^{-1}, with an average of 6×10^{-7} M$_{\odot}$ yr^{-1}. Therefore, while it seems objects possessing CO first overtone emission span a small range in mass accretion rate, their average mass accretion rate does not seem substantially different to objects without such CO emission.

The accretion rates are somewhat higher than measured by Calvet et al. (2004), who examined the spectra of nine intermediate-mass T Tauri stars and find an average mass accretion rate of 3×10^{-8} M$_{\odot}$ yr^{-1}. However, the HAeBes studied here are located at larger distances, are more luminous and are thus (on average) likely younger than the T Tauri stars described above. If mass accretion rates decrease with stellar age, then this may explain why the mass accretion rates of the HAeBes are higher than those of the T Tauri stars. When compared with similar objects, such as the study of 38 Herbig Ae stars by Mendigutía et al. (2011), the accretion rates determined here are in agreement with their reported median mass accretion rate of 2×10^{-7} M$_{\odot}$ yr^{-1}.

However, it should be noted that the relation in equation (4) was determined from examination of Herbig Ae objects (with $T_{\mathrm{eff}} < 1.2 \times 10^{4}$ K), and the applicability of this magnetospheric shock model in relation to the Herbig Be objects presented here has not yet been proven (Mendigutía et al. 2012). Other emission lines have been shown to accurately correlate with various emission excesses, allowing them to be used as accretion tracers (e.g. He I; Oudmaijer et al. 2011). This will be investigated in detail for the remainder of the X-shooter data set in a subsequent publication (Fairlamb et al., in preparation).

4 MODELLING THE CO BANDHEADS

In order to determine the origin of the CO emission, we fitted the spectra using a model describing the circumstellar environment of CO as a thin disc in Keplerian rotation, previously utilized in Wheelwright et al. (2010), Ilee et al. (2013) and Murakawa et al. (2013). The program is briefly described below.

The population of the CO rotational levels, to a maximum of $J = 100$, for each $\Delta v = 2$ vibrational transition considered are determined in each cell according to the Boltzmann distribution, which assumes local thermodynamic equilibrium, and a CO/H$_2$ ratio of 10^{-4}. The disc is divided into 75 radial and 75 azimuthal cells. Each transition is assumed to follow a Gaussian with a width of Δv. The intensity of emission from each cell of the disc is calculated from $I_{\nu} = B_{\nu}(T) \left(1 - e^{-\tau_{\nu}}\right)$. The emission is then assigned a weight determined from the solid angle subtended by the cell on the sky. The emission from each cell is wavelength shifted to account for the line-of-sight velocity due to the rotational velocity of the disc. The emission from all cells is then summed together, smoothed to the instrumental resolution and then shifted in wavelength to account for the radial velocity of the object to produce the entire CO bandhead profile for the disc.

The excitation temperature and surface number density of the disc are described analytically as decreasing power laws:

$$T(r) = T_{\mathrm{i}} \left(\frac{r}{R_{\mathrm{i}}} \right)^{p}, \qquad (6)$$

$$N(r) = N_{\mathrm{i}} \left(\frac{r}{R_{\mathrm{i}}} \right)^{q}, \qquad (7)$$

where T_{i} and N_{i} are the excitation temperature and surface density at the inner edge of the disc R_{i}, and p and q are the exponents describing the temperature and surface density gradient, respectively. The optical depth, τ, is taken to be the product of the absorption coefficient per CO molecule, and the CO column density. Since we are considering a geometrically thin disc, the column density is given by the surface number density N. The outer radius of the CO emission region is taken to be the radius at which T falls below 1000 K, the temperature at which we assume CO overtone emission can no longer be excited sufficiently to be detected.

The best-fitting model is determined using the downhill simplex algorithm, implemented by the AMOEBA routine of the IDL distribution. The input spectra are first continuum subtracted, and then

Table 4. Parameter space that is searched during the model fitting procedure.

Parameter	Range
Inclination i	$0° < i < 90°$
Intrinsic linewidth Δv	$1 < \Delta v < 30 \text{ km s}^{-1}$
Inner radius R_i	$1 < R_i < 100 \, R_\star$
Inner temperature T_i	$1000 < T_i < 5000 \text{ K}$
Inner surface density N_i	$10^{12} < N_i < 10^{25} \text{ cm}^{-2}$
Temperature exponent p	$-4 < p < 0$
Surface density exponent q	$-4 < q < 0$

normalized to the peak of the $v = 2$–0 bandhead. Model fits are compared to the data using the reduced chi-squared statistic, χ_r^2, and the error in the data is taken to be the standard deviation of the flux in the pre-bandhead portion of the spectra. Free parameters of the fit are the inner surface number density, the inner temperature, the inner radius, the intrinsic linewidth, the temperature and density exponents and the inclination. The fitting routine is repeated with six starting positions spread across the parameter space to avoid recovering only local minima in χ_r^2, and the final best-fitting model is determined from these six runs. The range of parameter space searched is shown in Table 4. Errors on the best-fitting parameters are calculated by holding all other fitting variables at their best-fitting values, and altering the parameter of interest until the difference in reduced chi-squared, $\Delta \chi_r^2$, increases by unity.

4.1 Fitting the X-shooter observations

The object HD 101412 provides useful test case for our analysis, as it has been observed with both X-shooter at medium resolution and CRIRES at high resolution. Fig. 4 shows the comparison of the $v = 2$–0 bandhead for both sets of observations.

The CRIRES spectrum at $R \sim 90\,000$ shows much detail that is not seen when the considering data of a lower spectral resolution of $R \sim 8000$. In particular, the individual rotational transitions in the blue shoulder of the bandhead and the double-peaked rotational transitions are almost entirely lost in the X-shooter spectrum. When the CRIRES spectrum is convolved with a Gaussian corresponding to the spectral resolution of the X-shooter data, re-binned the appropriate amount, and given a similar level of random noise, the data appear qualitatively similar to the X-shooter spectrum. However, measurement of the equivalent width of the original and degraded CRIRES spectra yielded very similar results (2.8 Å), while measurement of the X-shooter spectrum gave a larger equivalent width of 5.1 Å, suggesting that the CO first overtone emission in HD 101412 may be variable. Nonetheless, it is clear that much information is lost when the spectrum is degraded to the resolution of X-shooter.

We performed the fitting routine on both the high-resolution CRIRES data and the lower resolution X-shooter data for HD 101412. The fitting routine performed poorly on the X-shooter data, recovering multiple best-fitting solutions at similar χ_r^2 values with very different parameters (which we do not show here). We attribute this to the low-resolution data not showing important features in the spectra, such as the blue shoulder of the bandhead and the narrow, double-peaked rotational transitions mentioned earlier. However, when the fitting routine was performed on the high-resolution CRIRES spectra for HD 101412, a single, unambiguous best-fitting model was obtained.
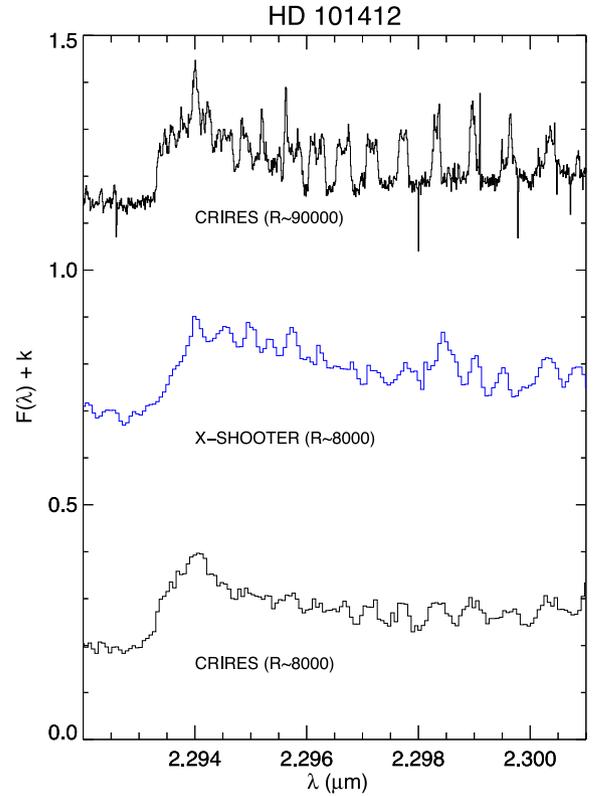
Figure 4. Comparison of CRIRES and X-shooter data for HD 101412. The CRIRES spectrum at $R \sim 90\,000$ shows much detail that is not distinguishable when considering data of a lower spectral resolution of $R \sim 8000$.

4.2 Fitting the CRIRES observations

Given the issues of fitting the X-shooter spectra described previously, we chose to restrict our modelling of the CO bandheads to the five objects observed with CRIRES. The results of this fitting are shown in Table 5 and Fig. 5. Below we discuss the fitting results on an object-by-object basis.

4.2.1 HD 36917

HD 36917 is assumed to be a B9.5 type, 2.5 $M_\odot$ star with a stellar radius of 1.8 $R_\odot$, an effective temperature of 10^4 K and located at a distance of 470 pc (Manoj et al. 2002; Brittain et al. 2007). The bolometric luminosity has been determined to be 245 $L_\odot$, with a visual extinction of 0.5 mag (Hamaguchi et al. 2005).

Our modelling of the CO bandheads indicates a best-fitting disc model extending from 0.1 to 1.5 au, at an inclination of 51°. The inner edge of the CO emitting region reaches a temperature of 3400 K, at a density of 6×10^{20} cm^{-2}. The temperature and surface number density exponents are well constrained at -0.5 and -1.8, respectively, and the temperature exponent agrees well with the value of -0.5 expected from a flat disc in radiative equilibrium (Chiang & Goldreich 1997). The location of the CO emission region crosses inside the dust sublimation radius of 0.4 au, as calculated from equation (1), but lies beyond the corotation radius of 0.02 au. The intrinsic linewidths of the individual transitions in the CO bandhead correspond to 5.4 km^{-1}, which are approximately 2–5 times the thermal linewidths for CO at temperatures between 1000 and 5000 K, indicating broadening by non-thermal mechanisms.

Table 5. Best-fitting parameters obtained from the fits to the CO overtone emission using the fitting routine. The outer disc radius is defined at the point in the disc in which the temperature drops below 1000 K, therefore, no error is presented. Errors shown with asterisks denote that the change in the value of the reduced chi-squared statistic χ_r^2 was less than one across the allowed parameter range used in the fitting procedure (see Table 4).

Output parameter		HD 36917	HD 259431	HD 58647	HD 101412	PDS 37
CO inner radius	R_i (au)	$0.1^{+0.01}_{-0.02}$	$0.89^{+0.1}_{-0.1}$	0.18 ± 0.01	$1.0^{+0.2}_{-0.1}$	$1.6^{+0.1}_{-0.5}$
CO outer radius	R_o (au)	1.5	4.3	0.62	1.1	3.8
Inclination	i (°)	51^{+7}_{-2}	52^{+5}_{-3}	75^{+*}_{-10}	87^{+*}_{-20}	89^{+*}_{-35}
Inner surface number density	N_i (cm^{-2})	$6.0^{+2}_{-3} \times 10^{20}$	$0.16^{+5.6}_{-*} \times 10^{20}$	$0.62^{+12}_{-*} \times 10^{20}$	$14^{+75}_{-4} \times 10^{21}$	$0.1^{+6.3}_{-*} \times 10^{20}$
Inner temperature	T_i (K)	3400^{+800}_{-250}	3200^{+10}_{-200}	2800^{+10}_{-300}	1000^{+50}_{-*}	5000^{+*}_{-1200}
Intrinsic linewidth	$\Delta \nu$ (km s^{-1})	5.4^{+3}_{-2}	$10.7 \pm *$	$10.8 \pm *$	5.2^{+3}_{-2}	$18 \pm *$
Temperature exponent	p	$-0.5^{+0.1}_{-0.1}$	$-0.74^{+0.4}_{-1.1}$	$-0.89^{+0.3}_{-0.9}$	$-0.46^{+*}_{-2.4}$	$-1.9^{+0.7}_{-*}$
Surface number density exponent	q	$-1.8^{+0.2}_{-0.2}$	$-3.3^{+1.2}_{-*}$	$-1.6^{+1.5}_{-*}$	$-0.5 \pm *$	$-1.7 \pm *$
Reduced chi-squared	χ_r^2	3.0	5.3	6.2	3.8	2.5

Our results are in contrast to the study of Berthoud (2008), who are unable to fit their observations of the CO $v = 2$–0 bandhead using a disc and/or ring model, due to the fitting procedure returning solutions that converge with unphysical values (such as temperatures higher than the dissociation temperature of CO). The authors therefore model the emission using an expanding shell of CO, which produces satisfactory fits to the spectrum, in particular the rounded, convex-shaped blue shoulder of the bandhead in their data. Our observations of HD 36917 do not exhibit such a rounded blue shoulder, but rather a traditional concave-shaped blue shoulder, traditionally attributed to emission from a disc. This allows us to obtain a satisfactory fit to the spectrum using our disc model. As our data are of higher spectral resolution than the observations presented in Berthoud (2008), it is unlikely that the differences in the spectrum presented here are due to a resolution effect. It is possible that the source of the CO emission in HD 36917 is variable, and that overtones are excited both within a disc and shell-like geometry around the central star. However, time monitoring of any spectral variability of the source would be required to confirm this.

4.2.2 HD 259431

HD 259431 (MWC 147) is taken to be a 6.6 M$_\odot$ star with a radius of 6.6 R$_\odot$, having a spectral type of B6, located at a distance of 800 pc. It has a high bolometric luminosity of 1550 L$_\odot$, and an effective temperature of 14 125 K (Kraus et al. 2008b).

The best-fitting disc model for HD 259431 extends from 0.89 to 4.3 au at an inclination of 52°. It is interesting to note that the spectrointerferometric study of Kraus et al. (2008b) determines an inclination of approximately 50° for this object, which agrees very well our derived disc inclination. The temperature and surface number density of the inner disc are 3000 K and 2×10^{20} cm^{-2}, with exponents of -0.7 and -3.3, respectively. The temperature exponent is in agreement with the expected value of -0.75 from a flat blackbody disc (Chiang & Goldreich 1997). The inner edge of the disc extends to within the dust sublimation radius of 3.3 au, however, this lies outside the corotation radius of 0.07 au as calculated from $v \sin i = 100$ km s^{-1} (Hillenbrand et al. 1992). The linewidth of the individual rotational transitions of CO is 10.7 km s^{-1}, however, this is not well constrained. Nevertheless, this is a factor of 3–8 times the thermal linewidth for CO at 1000–5000 K.

Brittain et al. (2007) measured the Brγ emission of HD 259431 and determine a full width at zero intensity (FWZI) of 350 km s^{-1},

with a luminosity of 38.1×10^{-4} L$_\odot$ which they calculate to correspond to a mass accretion rate of 4.1×10^{-7} M$_\odot$ yr^{-1} using a relationship based upon UV veiling. Using these measurements with the relationship described in Mendigutía et al. (2012), we calculate a higher mass accretion rate 3.2×10^{-6} M$_\odot$ yr^{-1}. Hillenbrand et al. (1992) also find a higher accretion rate of 1.01×10^{-5} M$_\odot$ yr^{-1}, determined from fitting the spectral energy distribution (SED) of HD 259431. This discrepancy may be explained by the fact that the accretion rate calibrations used have not been proven to be valid for Herbig Be stars as hot as HD 259431.

4.2.3 HD 58647

The stellar mass of HD 58647 is assumed to be 3.0 M$_\odot$ with a radius of 2.8 M$_\odot$, located at a distance of 277 pc (Brittain et al. 2007). It has an effective temperature of 10 500 K and a bolometric luminosity of 910 L$_\odot$ (Montesinos et al. 2009).

Minor issues were encountered while fitting HD 58647, which showed a decrease in SNR across the final detector chip containing the $v = 3$–1 bandhead. For this reason, the fitting routine was restricted to data from the first and second detector chip and extrapolated across the remaining data. Though this data are not included in the formal fitting process, it can be seen that the model qualitatively reproduces the features across this region of the spectrum very well.

The best-fitting model extends from 0.18 to 0.62 au, at an inclination of 75°. This is entirely within the dust sublimation radius of 1.1 au as calculated from equation (1). The inner edge of the CO emitting region reaches a temperature of 2800 K, at a density of 6.2×10^{19} cm^{-2}. The temperature and surface number density exponents are not well constrained, but give best-fitting values of -0.89 and -1.6, respectively. The intrinsic linewidths of the individual transitions in the CO bandhead correspond to 10.8 km s^{-1}, a factor of 3–8 times the thermal linewidth for CO at 1000–5000 K.

Berthoud (2008) fitted their observations of the CO overtone emission in HD 58647 with an optically thick ring at a temperature of 2380 K, a surface density of 1.6×10^{20} cm^{-2} and an intrinsic linewidth of 7.7 km s^{-1}, seen at a high inclination to the line of sight. These values agree with the fit obtained using our observations and disc model to within approximately 1–1.5σ. Brittain et al. (2007) measure the Brγ emission line from HD 58647 to be double peaked, with a FWZI of 400 km s^{-1}, and a luminosity of 21.8×10^{-4} L$_\odot$. They calculate this to correspond to an accretion
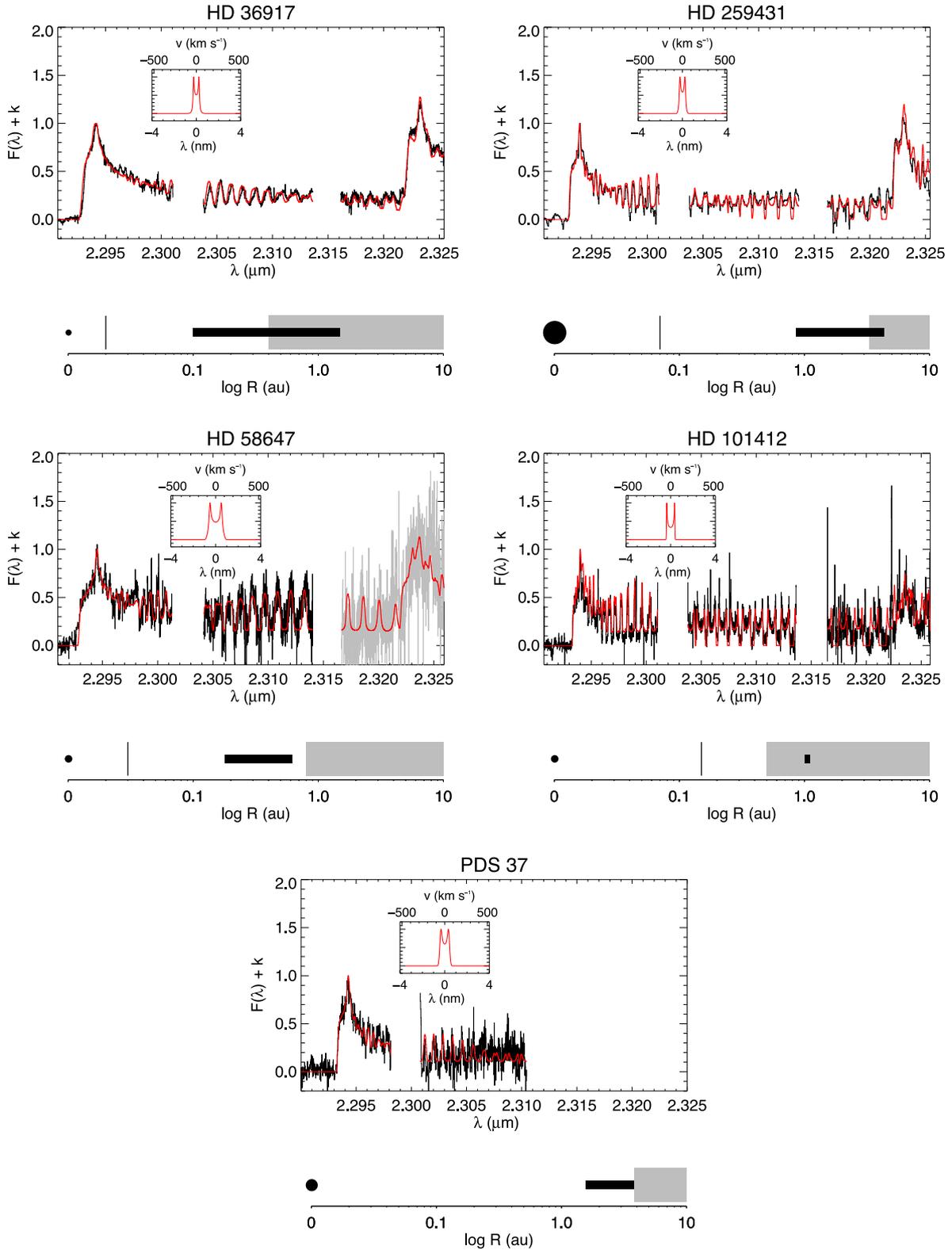
Figure 5. CRIRES spectra showing the CO first overtone bandhead emission (black) with best-fitting model (red). Regions of the spectrum excluded from the fitting are shown in grey. Insets show the line profile of the $J = 51$–50 transition of CO taken from the best-fitting model. Beneath the spectra are diagrams depicting the corresponding structure of the model: the size of the central star is shown at the origin, the black region depicts the size of the CO emission region, the grey region stretches from the dust sublimation radius outwards (equation 1) and a vertical line marks the location of the corotation radius (equation 2), where data are available.

rate of 3.5×10^{-7} M$_\odot$ yr^{-1}, which is consistent with the accretion rate of 4.8×10^{-7} M$_\odot$ yr^{-1} determined using equation (4).

4.2.4 HD 101412

We determine HD 101412 to be a 2.3 M$_\odot$ star with a radius of 2.2 R$_\odot$, and an effective temperature of 9750 K. It has a relatively low bolometric luminosity of 38 L$_\odot$, and a visual extinction of $A_V = 0.39$ mag. Our modelling of the CO overtone indicates a best-fitting disc model extending from 1.0 to 1.1 au, at an inclination of 87°. The inner edge of the CO emitting region reaches a relatively low temperature of 1000 K, at a relatively high density of 1.4×10^{22} cm^{-2}. The temperature and surface number density exponents are -0.46 and -0.5, respectively. These values are not well constrained, likely due to the fact that the emitting region is very narrow, and thus determination of a gradient for the temperature and density is difficult. The intrinsic linewidths of the individual transitions in the CO bandhead correspond to 5.2 km s^{-1}, which is 2–4 times the thermal linewidth. In contrast to all other best-fitting disc models, the CO emission region for HD 101412 lies beyond the dust sublimation radius of 0.5 au calculated from equation (1). Additionally, HD 101412 exhibits the relatively weak double-peaked Brγ emission, contrary to the strong single-peaked Brγ emission of other objects studied in this work.

HD 101412 was the subject of a similar investigation involving CO bandhead emission by Cowley et al. (2012). The authors find fits to their spectra assuming a disc of CO that is at most 0.8–1.2 au in extent, at a temperature of 2500 K, and assuming the disc is edge on, following the inclination of 80° determined from Fedele et al. (2008). Our results only differ slightly from Cowley et al. (2012), but it should be noted that their model and fitting routine were different to the methods presented here. For instance, they assume an isothermal ring of CO with fixed parameters such as inclination, and the fitting was performed visually with no systematic χ_r^2 minimization. However, the results here still suggest a narrow ring of CO, at approximately distance from the central protostar, at a slightly cooler temperature.

High spectral resolution observations of the [O I] emission line at 6300 Å were examined by van der Plas et al. (2008), who determined that this emission originates from a region in a disc from 0.15 to 10 au, viewed at an inclination of 30° and corresponds to a $v\sin i$ of 8 km s^{-1}. The authors suggest that HD 101412 is in transition between a flaring and self-shadowed disc. The authors also note a drop in the radial [O I] emission of 50 per cent at approximately 0.5 au (corresponding to their calculated dust sublimation radius), and a re-brightening shortly afterwards at approximately 0.8 au. The initial drop is attributed to the self-shadowing of a puffed up inner rim at the dust sublimation radius, but the authors note that the observed re-brightening is unexpected. HD 101412 was one of the subjects of a study of CO fundamental rovibrational emission by van der Plas (2010). The comparable linewidths of CO and [O I] led this author to suggest that HD 101412 has a disc with strongly flared gas, but mostly settled dust.

This interpretation could explain why we apparently detect CO bandhead emission beyond the dust sublimation radius in HD 101412, in contrast to the other objects studied here. Our best-fitting model for the spectrum of HD 101412 suggests a relatively cool (1000 K) but high-density (10^{22} cm^{-2}) emission environment – if there is a sufficient amount of dense gas located above the highly settled dust in the disc, then CO first overtone emission may originate from these regions. The X-shooter spectrum of HD 101412

only exhibits the CO $v = 2$–0 and 3–1 bandheads, suggesting there is not sufficient energy in the origin environment to excite the higher vibrational transitions.

It is not clear how our disc model would perform when attempting to fit CO emission that is not from an axisymmetric disc geometry, which may explain why our reported high inclination is in contrast to the low measured $v\sin i$ of 8 km s^{-1} and low inclination reported in van der Plas et al. (2008). In addition, as there is an inversely proportional degeneracy between the location of the emission and the disc inclination in our CO modelling procedure, adopting a lower inclination would mean the corresponding emission region is closer to the star, likely inside the dust sublimation radius. As the inclination recovered for HD 101412 is almost exactly edge on, then the reported location of the CO emission represents an upper limit to the radial distance of this region.

4.2.5 PDS 37

PDS 37 (also known as G282.2988$-$00.7769) was previously investigated as a massive young stellar object in Ilee et al. (2013), where a stellar mass, radius and effective temperature of 11.8 M$_\odot$ and 4.7 R$_\odot$, 26 100 K were calculated from the bolometric luminosity and adopted for the fitting of the CO emission. This lead to a best-fitting disc model 1.7–9 au in extent, at an inclination of 80°. The inner temperature of the disc was 4800 K, and the surface density was 1×10^{20} cm^{-2}, varying with a slope of -0.97 and -1.4, respectively. The intrinsic linewidth of the transitions was determined to be 16.3 km s^{-1}.

Here we calculate PDS 37 to have a mass of 7.0 M$_\odot$, a radius of 3.0 R$_\odot$, a bolometric luminosity of 1860 L$_\odot$ and an effective temperature of 22 000 K. Modelling the CO bandhead emission using these stellar parameters indicates a best-fitting disc model extending from 1.6 to 3.8 au, at an inclination of 89^{+1}_{-35} °. The inner edge of the CO emitting region reaches a temperature of 5000 K, at a density of 1.0×10^{19} cm^{-2}. The temperature and surface number density exponents are not well constrained at -1.9 and -1.7, respectively. The location of the CO emission region coincides with dust sublimation radius of 1.5 au, as calculated from equation (1). The intrinsic linewidths of the individual transitions in the CO bandhead correspond to 18 km s^{-1}, which is approximately 6–14 times the thermal linewidths for CO at temperatures between 1000 and 5000 K. Altering the stellar parameters changes the best-fitting model parameters slightly, however, still indicates a relatively large CO emission region, at a high temperature, viewed almost edge-on.

PDS 37 is also the subject of a spectropolarimetric study by Ababakr et al. (in preparation), where strong polarization signatures are seen across the Hα and doubly-peaked Fe II emission lines, indicating the presence of a gaseous disc viewed at a high inclination to the line of sight.

5 DISCUSSION

5.1 The detection rate of CO first overtone emission

From an initial sample of 90 targets obtained with X-shooter (the most complete spectroscopic sample of Herbig Ae/Be stars to date), we find a low detection rate of CO first overtone bandhead emission of approximately 7 per cent. While a low detection rate in itself is in agreement with previous studies, our detection rate is substantially lower than studies of low-mass T Tauri and Herbig Ae stars (20 per cent; Carr 1989; Connelley & Greene 2010), and also of higher mass MYSOs (17 per cent; Cooper et al. 2013).

It is also striking that although our full X-shooter sample contains many A-type stars, we have only detected CO overtone emission in one A-type star. In contrast to this, although our sample contains few B- and F-type stars, we have detected CO in a total of seven B-type stars and one F-type star. So, also in our sample there may be evidence that the detection rate for CO first overtone emission is lower for intermediate-mass young stars than for low- and high-mass young stars. Below we discuss possible explanations for this.

High temperatures are required to excite the CO sufficiently in order for CO bandhead emission to become detectable. Several of the objects in our study are B-type stars (and HD 101412 is of type HA0, having also been classified as B-type by Manoj et al. 2006). Therefore, these objects are hotter and more massive than their A-type counterparts. It could be that many T Tauri and Herbig Ae stars are not hot enough to continually excite the CO overtones in a circumstellar disc environment. In such cases, variable CO emission in lower mass YSOs could be explained by bursts of active accretion (Biscaya et al. 1997) or by originating from a different environment (e.g. magnetic funnel flows; Martin 1997). However, modelling of high spectral resolution observations of a large number of T Tauri stars would be required to confirm the origin of the emission.

It is also possible that the majority HAeBes do not have enough gas in their close circumstellar environments to allow sufficient excitation of the CO bandheads. In addition to high temperatures, high densities ($n > 10^{15}$ cm^{-3}) are required before this rovibrational emission becomes sufficiently excited to be detectable. While direct measurements of the amount of gas within these young stellar systems are difficult, there is evidence of cleared gaps around many HAeBe stars (a recent example being HD 142527; Casassus et al. 2012). If the gas within these inner regions is cleared efficiently, then it will not be possible to reach densities high enough to allow overtone emission to occur. Our modelling of the CO overtone spectra indicates the emission originates from environments with a surface density of at least 10^{20} cm^{-2}. In addition, Muzerolle et al. (2004) present models of the inner regions of discs around HAeBe stars, and show that for accretion rates greater than 10^{-8} M$_{\odot}$ yr^{-1}, the inner gaseous disc becomes optically thick. The accretion rates determined from our analysis of the Brγ in these objects are above this level, further suggesting that these objects possess a large amount of gas of a high density close to the central protostar.

One unresolved issue with this interpretation is that there are a handful of objects possessing high accretion rates that do not exhibit CO first overtone emission. The work of Calvet et al. (1991) showed that CO in absorption could be expected from high mass accretion rates (observed in FU Ori objects), however, we do not detect such absorption in our observations.

5.2 The location and orientation of the emitting regions

The location of the detected emission is of interest, as it determines which regions of the circumstellar environment can be probed. We find that four out of five of the objects possess best-fitting disc models with inner radii located interior to the corresponding dust sublimation radii. This suggests that the CO emission originates from a gaseous disc, close to the central protostar. The one object for which this is not the case, HD 101412, exhibits features which are not typical when compared to the other objects studied here (see Section 4.2.4).

The corotation radii lie between 0.02 and 0.23 au, and are interior to the dust sublimation radius in all objects. The CO emission is also shown to originate from beyond the corotation radius, in objects where $v\sin i$ measurements are available in the literature. Therefore,

our modelling suggests that while CO first overtone emission is a valuable probe of the inner gaseous disc component around young stars, other spectral tracers are required to trace regions close to the corotation radius, where any deviations from magnetospheric accretion geometry are likely to occur.

The inclinations of the best-fitting disc models range from 51° to 72°, suggesting a preference for moderate to high inclinations. While the number of objects modelled in this paper is too low to accurately determine the statistical significance of this, it is nonetheless possible that a geometric selection effect is at work. One possible explanation for a preference towards more inclined discs could be that in addition to a inner disc, the CO emission may also trace the vertical inner wall of dust disc, located at the dust sublimation radius. However, further investigation using models that are able to include such emission geometry would be required to confirm this.

A preference for moderate to high inclinations is in contrast to the study of CO emission of massive YSOs by Ilee et al. (2013), which found an essentially random orientation of disc inclinations. The masses of the objects studied in Ilee et al. (2013) were determined from the bolometric luminosity of the objects, which may have included contributions from accretion, and could therefore be overestimates of the true stellar masses. In such cases, an overestimate of the stellar mass can lead to a lower inclination being recovered. This effect can be seen in our modelling of PDS 37 – in this work, we recover a an inclination of 87° using a stellar mass of 7.0 M$_{\odot}$, while in Ilee et al. (2013) we recover an inclination of 80° from a stellar mass of 12 M$_{\odot}$. While this effect is small, it may explain why no such preference for moderate- to high-inclination angles was found for MYSOs.

A positive correlation between the line luminosities of the CO bandhead and Brγ is found, and while this does not imply a direct dependence (and the number of objects with emission is too low to attribute a statistical significance to the correlation), it does suggest that similar factors affect the strength of both emission lines. However, analysis of the linewidths shows that the Brγ emission is approximately 20 times larger than the corresponding linewidths obtained from the fitting of the CO bandheads. This difference in linewidth suggests that both lines do not originate in the same kinematic environment, and are therefore likely not cospatial. This is in contrast to the recent interferometric study of Eisner, Hillenbrand & Stone (2014), who find a near-coincidence of CO overtone, Brγ and continuum emission in five YSOs. The spectrointerferometric study of Kraus et al. (2008a) suggests two possible origins for Brγ emission – compact regions, or more extended regions possibly tracing stellar or disc winds. Further analysis on the precise location of the Brγ emission will be required in order to study any possible connections between these two emission lines.

6 CONCLUSIONS

This paper presents medium-resolution VLT/X-shooter and high-resolution VLT/CRIRES NIR spectra of several Herbig Ae/Be stars, in an investigation of the inner regions of their circumstellar discs. Below we summarize the main findings.

(i) From a large spectroscopic survey of over 90 HAeBe targets, we detect only six objects exhibiting CO first overtone bandhead emission, corresponding to a detection rate of approximately 7 per cent. Analysis of the upper limits suggests that the majority of non-detections are not due to the sensitivity of the X-shooter instrument.

(ii) The objects displaying CO overtone emission are mainly of spectral type B, and are thus hotter and more massive than their A-type counterparts.

(iii) In all objects that display CO bandhead emission, we also find Brγ emission of varying strengths. We find a positive correlation between the strength of the CO $v = 2$–0 bandhead and the Brγ line, in agreement with previous investigations (Carr 1989; Connelley & Greene 2010), showing this correlation extends to YSOs of higher masses.

(iv) The high-resolution spectra of five objects exhibiting CO first overtone emission are fitted with a model of a thin disc undergoing Keplerian rotation, and good fits are obtained to all spectra. It was determined that the spectral resolution of the X-shooter instrument was insufficient to obtain reliable model fits using this procedure.

(v) The linewidths of the Brγ emission are between 10 and 40 times larger than the intrinsic linewidths of the CO overtone emission, suggesting that they originate in different kinematic environments.

(vi) The location of the CO overtone emission in these best-fitting models is consistent with the hypothesis that it originates from a small-scale gaseous disc, interior to the dust sublimation radius, but beyond the corotation radius of the central star.

It is important to note that for the object where spatially resolved observations have also been performed, HD 259431 (MWC 147; Kraus et al. 2008b), we obtain a remarkably similar value to the inclination of the disc based on our fitting technique ($\sim$50°). While this comparison can currently only be made in one object, it does suggest that high spectral resolution observations can be used as an alternative to interferometric observations to investigate the sub-au scale regions around young stars.

We plan to investigate this with further observations using VLT Interferometer/Astronomical Multibeam Combiner (AMBER), which will enable direct measurements of the spatial extent of the CO emitting gas, and allow comparison with our spectral fitting technique. This, alongside more sophisticated modelling that can include the vertical structure of inner discs, will provide much information on the nature of the inner regions around Herbig Ae/Be stars.

ACKNOWLEDGEMENTS

REFERENCES

Alecian E. et al., 2013, MNRAS, 429, 1001
Berthoud M. G., 2008, PhD thesis, Cornell University
Bertout C., 1989, ARA&A, 27, 351
Bertout C., Basri G., Bouvier J., 1988, ApJ, 330, 350
Bik A., Thi W. F., 2004, A&A, 427, L13
Biscaya A. M., Rieke G. H., Narayanan G., Luhman K. L., Young E. T., 1997, ApJ, 491, 359
Blondel P. F. C., Tjin A Djie H. R. E., 2006, A&A, 456, 1045
Blum R. D., Barbosa C. L., Damineli A., Conti P. S., Ridgway S., 2004, ApJ, 617, 1167
Bouvier J., Alencar S. H. P., Harries T. J., Johns-Krull C. M., Romanova M. M., 2007, in Reipurth B., Jewitt D., Keil K., eds, Protostars and Planets V. University of Arizona Press, Tucson, p. 479
Bressan A., Marigo P., Girardi L., Salasnich B., Dal Cero C., Rubele S., Nanni A., 2012, MNRAS, 427, 127
Brittain S. D., Simon T., Najita J. R., Rettig T. W., 2007, ApJ, 659, 685
Calvet N., Patino A., Magris G. C., D'Alessio P., 1991, ApJ, 380, 617
Calvet N., Muzerolle J., Briceño C., Hernández J., Hartmann L., Saucedo J. L., Gordon K. D., 2004, AJ, 128, 1294
Cardelli J. A., Clayton G. C., Mathis J. S., 1989, ApJ, 345, 245
Carr J. S., 1989, ApJ, 345, 522
Casassus S., Perez M. S., Jordán A., Ménard F., Cuadra J., Schreiber M. R., Hales A. S., Ercolano B., 2012, ApJ, 754, L31
Castelli F., Kurucz R. L., 2004, preprint (arXiv Astrophys. e-prints)
Chiang E. I., Goldreich P., 1997, ApJ, 490, 368
Connelley M. S., Greene T. P., 2010, AJ, 140, 1214
Cooper H. D. B. et al., 2013, MNRAS, 430, 1125
Cowley C. R., Hubrig S., Castelli F., Wolff B., 2012, A&A, 537, L6
de Zeeuw P. T., Hoogerwerf R., de Bruijne J. H. J., Brown A. G. A., Blaauw A., 1999, AJ, 117, 354
Dullemond C. P., Monnier J. D., 2010, ARA&A, 48, 205
Eisner J. A., Hillenbrand L. A., Stone J. M., 2014, MNRAS, 443, 1916
Fedele D. et al., 2008, A&A, 491, 809
Ferreira J., 1997, A&A, 319, 340
Folha D. F. M., Emerson J. P., 2001, A&A, 365, 90
Garcia Lopez R., Natta A., Testi L., Habart E., 2006, A&A, 459, 837
Glassgold A. E., Najita J., Igea J., 2004, ApJ, 615, 972
Guimarães M. M., Alencar S. H. P., Corradi W. J. B., Vieira S. L. A., 2006, A&A, 457, 581
Hamaguchi K., Yamauchi S., Koyama K., 2005, ApJ, 618, 360
Hillenbrand L. A., Strom S. E., Vrba F. J., Keene J., 1992, ApJ, 397, 613
Hubrig S., Schöller M., Savanov I., Yudin R. V., Pogodin M. A., Štefl S., Rivinius T., Curé M., 2009, Astron. Nachr., 330, 708
Ilee J. D. et al., 2013, MNRAS, 429, 2960
Käufl H. U. et al., 2008, Proc. SPIE, 7014, 70140W
Kraus S. et al., 2008a, A&A, 489, 1157
Kraus S., Preibisch T., Ohnaka K., 2008b, ApJ, 676, 490
Kurucz R. L., 1993, Kurucz CD-ROM. Smithsonian Astrophysical Observatory, Cambridge, MA
Larson R. B., 2003, Rep. Progress Phys., 66, 1651
Lynden-Bell D., Pringle J. E., 1974, MNRAS, 168, 603
McKee C. F., Ostriker E. C., 2007, ARA&A, 45, 565
Manoj P., Maheswar G., Bhatt H. C., 2002, MNRAS, 334, 419
Manoj P., Bhatt H. C., Maheswar G., Muneer S., 2006, ApJ, 653, 657
Martin S. C., 1997, ApJ, 478, L33
Mendigutía I., Calvet N., Montesinos B., Mora A., Muzerolle J., Eiroa C., Oudmaijer R. D., Merín B., 2011, A&A, 535, A99
Mendigutía I., Mora A., Montesinos B., Eiroa C., Meeus G., Merín B., Oudmaijer R. D., 2012, A&A, 543, A59
Miroshnichenko A. S., Levato H., Bjorkman K. S., Grosso M., 2001, A&A, 371, 600
Miroshnichenko A. S., Gray R. O., Klochkova V. G., Bjorkman K. S., Kuratov K. S., 2004, A&A, 427, 937
Modigliani A. et al., 2010, Proc. SPIE, 7737, 773728
Monnier J. D., Millan-Gabet R., 2002, ApJ, 579, 694
Montesinos B., Eiroa C., Mora A., Merín B., 2009, A&A, 495, 901
Mora A. et al., 2001, A&A, 378, 116
Mottram J. C., Vink J. S., Oudmaijer R. D., Patel M., 2007, MNRAS, 377, 1363
Murakawa K., Lumsden S. L., Oudmaijer R. D., Davies B., Wheelwright H. E., Hoare M. G., Ilee J. D., 2013, MNRAS, 436, 511
Muzerolle J., Calvet N., Hartmann L., 1998a, ApJ, 492, 743
Muzerolle J., Hartmann L., Calvet N., 1998b, AJ, 116, 2965
Muzerolle J., Calvet N., Hartmann L., D'Alessio P., 2003, ApJ, 597, L149
Muzerolle J., D'Alessio P., Calvet N., Hartmann L., 2004, ApJ, 617, 406
Oudmaijer R. D. et al., 2001, A&A, 379, 564
Oudmaijer R. D. et al., 2011, Astron. Nachr., 332, 238
Reipurth B., Zinnecker H., 1993, A&A, 278, 81

Shu F., Najita J., Ostriker E., Wilkin F., Ruden S., Lizano S., 1994, ApJ, 429, 781

Skrutskie M. F. et al., 2006, AJ, 131, 1163

Strafella F., Pezzuto S., Corciulo G. G., Bianchini A., Vittone A. A., 1998, ApJ, 505, 299

Tatulli E. et al., 2008, A&A, 489, 1151

Thé P. S., de Winter D., Perez M. R., 1994, A&AS, 104, 315

Thi W.-F., van Dalen B., Bik A., Waters L. B. F. M., 2005, A&A, 430, L61

Turner N. J., Fromang S., Gammie C., Klahr H., Lesur G., Wardle M., Bai X.-N., 2014, preprint (arXiv e-prints)

Tuthill P. G., Monnier J. D., Danchi W. C., 2001, Nature, 409, 1012

van den Ancker M. E., de Winter D., Tjin A Djie H. R. E., 1998, A&A, 330, 145

van der Plas G., 2010, PhD thesis, Univ. Amsterdam

van der Plas G., van den Ancker M. E., Fedele D., Acke B., Dominik C., Waters L. B. F. M., Bouwman J., 2008, A&A, 485, 487

van Leeuwen F., 2010, Space Sci. Rev., 151, 209

Vernet J. et al., 2011, A&A, 536, A105

Vieira S. L. A., Corradi W. J. B., Alencar S. H. P., Mendes L. T. S., Torres C. A. O., Quast G. R., Guimarães M. M., da Silva L., 2003, AJ, 126, 2971

Vink J. S., Drew J. E., Harries T. J., Oudmaijer R. D., Unruh Y. C., 2003, A&A, 406, 703

Vink J. S., Drew J. E., Harries T. J., Oudmaijer R. D., Unruh Y., 2005, MNRAS, 359, 1049

Wall J. V., Jenkins C. R., 2003, Practical Statistics for Astronomers. Cambridge Univ. Press, Cambridge

Waters L. B. F. M., Waelkens C., 1998, ARA&A, 36, 233

Wheelwright H. E., Oudmaijer R. D., de Wit W. J., Hoare M. G., Lumsden S. L., Urquhart J. S., 2010, MNRAS, 408, 1840

Wheelwright H. E., de Wit W. J., Weigelt G., Oudmaijer R. D., Ilee J. D., 2012, A&A, 543, A77

Whitney B. A., Indebetouw R., Bjorkman J. E., Wood K., 2004, ApJ, 617, 1177

Wood K., Lada C. J., Bjorkman J. E., Kenyon S. J., Whitney B., Wolff M. J., 2002, ApJ, 567, 1183

This paper has been typeset from a TEX/LATEX file prepared by the author.